

# Resource-efficient linear-optical generation of GHZ-like states

Suren A. Fldzhyan,<sup>1,2,\*</sup> Stanislav S. Straupe,<sup>3,1,2</sup> and Mikhail Yu. Saygin<sup>3,2</sup>

<sup>1</sup>*Russian Quantum Center, Bolshoy bul'var 30 building 1, Moscow, 121205, Russia*

<sup>2</sup>*Faculty of Physics, M. V. Lomonosov Moscow State University, Leninskie Gory 1, Moscow, 119991, Russia*

<sup>3</sup>*Sber Quantum Technology Center, Kutuzovskiy prospect 32, Moscow, 121170, Russia*

(Dated: November 10, 2025)

Heralded multi-photon entanglement generation is a central bottleneck for photonic quantum computing, where resource costs typically skyrocket with target size. We explore efficient methods for generating photon states with tunable entanglement, providing a flexible tool for quantum state engineering. We introduce a theoretical framework that has been numerically validated, demonstrating the capacity to generate GHZ-like states incrementally from non-logical intermediate states. We demonstrate that in certain scenarios – such as reducing the resource cost for building large maximally entangled GHZ states – these variable-entanglement states can outperform their fixed-entanglement counterparts. By adjusting intermediate states and optimizing interferometer schemes, we improve photon number cost efficiency of GHZ-like states generation. Our findings indicate that while not a universal solution, non-maximally entangled states offer practical advantages for specific photonic quantum information tasks.

## I. INTRODUCTION

Photonic platform is one of the leading route of quantum information processing because interference, detection, and feed-forward can be realized with mature linear-optical hardware. In particular, it is now widely regarded as a promising route to demonstrating quantum advantage [1–3]. Several quantum computing architectures tailored to discrete photons propagating through linear-optical interferometers and being measured have been proposed [4–7], including the fusion-based quantum computing (FBQC) model [7–10].

To realize FBQC, one must impart a preliminary large network of entangled qubits even before initiating the actual programmable quantum computation. Useful photon entanglement can be generated through photon interactions, either via matter-mediated processes [11–17], or by partially measuring freely interfering photons [4, 18, 19]. This paper focuses on the latter approach, which underpins measurement-induced entanglement generation.

Realizing FBQC requires generating a seed entangled photon states, with Greenberger-Horne-Zeilinger (GHZ) states – maximally entangled multipartite states – serving as critical resources for universal photonic quantum computation. Yet producing them with high efficiency remains challenging due to the probabilistic nature of linear-optical operations, detector loss, and rapidly growing resource overheads with target size. Our primary motivation is to improve methods for creating resource states for FBQC.

Heralded entangled state generation is a key criterion for robustness against photon losses [20]. Recent experimental demonstrations of heralded 2- and 3-qubit photonic entangled states [21, 22] have largely been guided

by proposals derived from numerical optimization of Fock space states transformation [23–28]. While these numerical methods produce highly efficient protocols, they often do not scale well to larger photon numbers. This underscores the importance of proposing architectures that support the systematic generation of entangled states at scale [29–32].

The primate-based fusion framework and the bleeding technique introduced by Bartolucci *et al.* [29], have made significant progress by using intermediate entangled states (called “primates”) that are progressively fused to produce arbitrarily large entangled states. However, these methods typically assume fixed entanglement parameters, limiting their adaptability for generating non-maximally entangled or tunable target states. This limitation motivates the development of more flexible strategies.

In this work, we extend the primate fusion technique of [29] to develop a framework for generating GHZ-like states with variable entanglement. Unlike prior approaches that focus on maximally entangled states, our method incorporates non-maximally entangled primate states in intermediate steps, leading to reduced photon resource costs — even when the target is a maximally entangled GHZ state — without sacrificing generation probability. The photon resource cost we consider is defined as the average number of photons required to produce a single target state.

By varying the entanglement in primate states, we achieve explicit control over the entanglement parameter  $s$  in the generation of  $N$ -qubit GHZ-like states, defined as  $|\text{GHZ}_N(s)\rangle = \sqrt{s}|10\rangle^N + \sqrt{1-s}|01\rangle^N$ . Through optimization over the entanglement degrees of primate states, we demonstrate a reduction in photon resource costs while maintaining the flexibility to produce target states with arbitrary entanglement.

Our framework is validated through numerical optimizations, which show variable-entanglement primates can outperform fixed-entanglement approaches in effi-

\* E-mail me at: [fldzhya@my.msu.ru](mailto:fldzhya@my.msu.ru)

ciency. For example, generating the maximally entangled GHZ state,  $|\text{GHZ}_N(0.5)\rangle$ , requires fewer photons when intermediate states with tunable entanglement are employed. This underscores the practical benefits of integrating adjustable entanglement into state-generation protocols of photonic quantum computing.

The bleeding technique [29] provides a strategy to further reduce the resource costs of state generation. This approach is conceptually linked to fundamental photon state engineering techniques in quantum optics [33, 34]. A canonical example involves repeatedly passing an input state through one port of a highly transmissive beam-splitter – with vacuum injected into the other – and measuring the output; a successful single-photon detection heralds the implementation of photon subtraction via an annihilation operator [35, 36].

In this work, we also refine the bleeding technique, in which photons propagate through linear-optical circuits until specific measurements are performed, followed by post-selection and corrections. We introduce a non-exhaustive bleeding protocol, in which the degree of photon retention during the process is treated as a tunable parameter that controls the generation efficiency. For large-scale implementations, we show that constant beamsplitter transmittances can approximate optimal resource scaling, thereby reducing experimental complexity. We demonstrate that this approach leads to a significant reduction in the overall resource cost.

This paper is structured as follows: Section II reviews foundational concepts. Section III revisits the primate-based fusion framework and introduces our modifications. Section IV details the adapted bleeding procedure. Finally, Section V discusses implications and potential applications.

## II. BASIC CONCEPTS

### A. Linear-optical evolution

The state of photons in the Fock space [37] is described as a superposition of terms involving photon creation operators. For  $M$  modes, a pure state takes the form:

$$|\psi\rangle = \sum_{\mathbf{T}} \alpha_{\mathbf{T}} |T_1, \dots, T_M\rangle = \sum_{\mathbf{T}} \frac{\alpha_{\mathbf{T}}}{\sqrt{\prod_{j=1}^M T_j!}} \hat{a}_1^{\dagger T_1} \dots \hat{a}_M^{\dagger T_M} |\text{vac}\rangle, \quad (1)$$

where  $|T_1, \dots, T_M\rangle$  represents the Fock basis with  $T_j$  photons in mode  $j$ .

Linear optical evolution is governed by a unitary operator  $\hat{U}$ , which corresponds to an  $M \times M$  interferometer matrix  $U$ . The evolved state  $\hat{U}|\psi\rangle$  is obtained by appropriately inserting  $\hat{U}\hat{U}^\dagger$  into each term of the superposition (1). Under this transformation, the photon creation

operators evolve as:

$$\hat{U}\hat{a}_i^{(\text{in})\dagger}\hat{U}^\dagger = \sum_{j=1}^M \hat{a}_j^{(\text{out})\dagger} U_{ji}, \quad (2)$$

and the vacuum state remains invariant,  $\hat{U}|\text{vac}\rangle = |\text{vac}\rangle$ . These properties simplify state evolution for low photon numbers. For notational simplicity, we will omit explicit (in) and (out) labels where no ambiguity arises.

The interferometer matrix  $U$  is constructed by multiplying elementary components matrices. For instance, a beamsplitter with transmittance  $t$  is represented by:

$$\begin{pmatrix} \sqrt{t} & \sqrt{1-t} \\ \sqrt{1-t} & -\sqrt{t} \end{pmatrix}, \quad (3)$$

and a phase shifter applying  $e^{i\phi}$  to mode 1 is:

$$\begin{pmatrix} e^{i\phi} & 0 \\ 0 & 1 \end{pmatrix}. \quad (4)$$

These components are sufficient to synthesize any unitary interferometer matrix  $U$  [38].

To determine the post-measurement state  $|\psi'\rangle$  after photon detection, we apply the measurement projector  $\hat{\mathcal{M}}$  to the input state:

$$|\psi'\rangle = \hat{\mathcal{M}}|\psi\rangle, \quad (5)$$

where  $\|\psi'\|^2$  gives the probability of the measurement outcome. For example, a measurement of  $k$  photons at mode  $i$  corresponds to the projector  $\hat{\mathcal{M}}_i^{(k)} = |k\rangle_i \langle k|_i$ . Since photon measurements destroy the detected photons, the projector can be more compactly written as:

$$\hat{\mathcal{M}}_i^{(k)} = \langle k|_i = \langle \text{vac} | \frac{\hat{a}_i^k}{\sqrt{k!}}, \quad (6)$$

where  $\hat{a}_i$  is the annihilation operator for mode  $i$ . This form simplifies the notation and is particularly useful when analyzing measurement-induced state transformations.

A practical tool for describing state transformation after measurement is backpropagation. When measuring a state after unitary evolution  $\hat{U}$ , the effect of the evolution can be transferred to the measurement operator:

$$\begin{aligned} \langle k|_i \hat{U}|\psi\rangle &= \langle \text{vac} |_i \hat{U} \frac{(\hat{U}^\dagger \hat{a}_i^{(\text{out})} \hat{U})^k}{\sqrt{k!}} |\psi\rangle = \\ &= \langle \text{vac} |_i \hat{U} \frac{(\sum_{j=1}^M U_{ij} \hat{a}_j^{(\text{in})})^k}{\sqrt{k!}} |\psi\rangle, \end{aligned} \quad (7)$$

and then using the algebra of input ladder operators to simplify state for (in) operators before evolving them to (out). This technique simplifies the analysis by partially shifting the complexity of the unitary evolu-

tion to the measurement operator, enabling in some cases a more straightforward description of the post-measurement state.

### B. Fusion

The fusion operation enables the introduction of entanglement between two initially separable photon states. This process involves performing partial measurements on photons from each state to herald the creation of a larger entangled state [4]. In our framework, the fusion unit  $F^{(t)}$  operates on a pair of modes in the setup depicted in Figure 1, where a beamsplitter between two modes is represented by a vertical line with points at the edges. The fusion is considered successful when exactly one photon is measured across the detectors. This process can be fine-tuned by adjusting the beamsplitters' transmittance parameters  $t$ .

Using the backpropagation outlined in Section II A we can recover the measurement operators for different cases. The measurement operators  $\hat{\mathcal{M}}_{ij}^{(\text{vac})}$  for measuring zero or  $\hat{\mathcal{M}}_{ij}^{(10)}$  &  $\hat{\mathcal{M}}_{ij}^{(01)}$  for measuring single photon are:

$$\hat{\mathcal{M}}_{ij}^{(\text{vac})} = \sqrt{t\hat{\mathcal{N}}_{ij}}, \quad (8)$$

$$\hat{\mathcal{M}}_{ij}^{(10) \text{ or } (01)} = \sqrt{\frac{t\hat{\mathcal{N}}_{ij}(1-t)}{2}} (\hat{a}_i \pm \hat{a}_j), \quad (9)$$

where  $\hat{\mathcal{N}}_{ij} = \hat{a}_i^\dagger \hat{a}_i + \hat{a}_j^\dagger \hat{a}_j$ .

We note that a technique known as boosting can be used to increase the fusion success probability [6, 39, 40]. While we believe that incorporating boosting could further reduce resource costs, we do not include it in our analysis for the sake of simplicity.

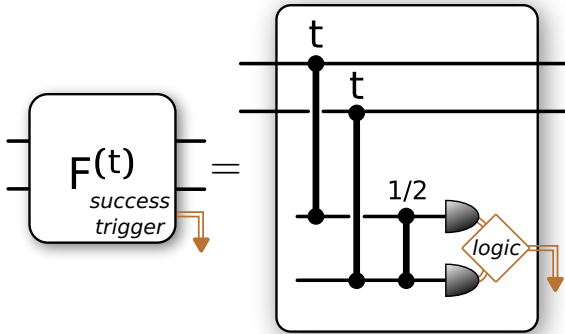


FIG. 1. Schematic of the fusion unit. A success trigger can be added to sum detector signals and output a signal when only one photon is detected. Copper wires represent classical signals, with arrows indicating direction. The logical unit discriminates single-photon detection and sends the corresponding signal.

## III. PRIMATE TRANSFORMATION

### A. Primates

The work [29] introduced the framework of “primate” states — specialized photonic resource states that enable the stepwise construction of maximally entangled GHZ states via successive fusion operations. Here, we generalize this construction by introducing a broader family of primates. Formally, we define a variable primate state as a pure state of  $n + 1$  photons distributed across  $2n$  modes, denoted  $|\pi^{(n)}(\lambda, s)\rangle$ , and parameterized by two continuous variables  $\lambda$  and  $s$ . Its explicit form is

$$|\pi^{(n)}(\lambda, s)\rangle = \sqrt{\lambda}|s^{(n)}\rangle + \sqrt{1-\lambda}|0\rangle|\zeta\rangle|0\rangle, \quad (10)$$

$$|s^{(n)}\rangle = \sqrt{s}|2\rangle|01\rangle^{n-1}|0\rangle + \sqrt{1-s}|0\rangle|10\rangle^{n-1}|2\rangle, \quad (11)$$

where  $|\zeta\rangle$  is a normalized state of  $n + 1$  photons in  $2n - 2$  modes. Informally,  $s$  sets the entanglement strength, while  $\lambda$  gives the weight of the useful component relative to the junk component. The outermost modes of a primate state are designated for fusion and measurement; the internal modes remain isolated from subsequent interactions.

Our procedure begins with a generation of initial primate states  $|\pi^{(1)}(1, s)\rangle = |s^{(1)}\rangle = \sqrt{s}|20\rangle + \sqrt{1-s}|02\rangle$ . When  $s = 1/2$ , the state  $\frac{|20\rangle + |02\rangle}{\sqrt{2}}$  can be deterministically created by passing  $|11\rangle$  through a balanced beamsplitter. However, generating  $|\pi^{(1)}(1, s)\rangle$  from two single photons for arbitrary  $s$  is not deterministic [41, 42].

To generate  $|\pi^{(1)}(1, s)\rangle$  we employ the scheme presented in Figure 2. For  $s \geq 1/2$ , one can use a beamsplitter between the second mode and an ancilla mode with transmittance  $\sqrt{\frac{1-s}{s}}$ . After performing a vacuum measurement on the ancilla, the resulting state is:

$$\frac{|20\rangle + \sqrt{\frac{1-s}{s}}|02\rangle}{\sqrt{2}} = \frac{1}{\sqrt{2s}}|\pi^{(1)}(1, s)\rangle, \quad (12)$$

with success probability  $\frac{1}{2s}$ . Additionally, detecting a single photon in the ancilla mode heralds the presence of a single photon, which can be recycled as a resource. The probability of recycling a single photon is given by  $\sqrt{\frac{1-s}{s}} \left(1 - \sqrt{\frac{1-s}{s}}\right)$ . Using these probabilities, we derive the average photon cost  $\nu^{(1)}$  for generating  $|\pi^{(1)}(1, s)\rangle$  as:

$$\nu^{(1)}(s) = 4s - 2\sqrt{1-s}(\sqrt{s} - \sqrt{1-s}). \quad (13)$$

If  $s < 1/2$ , the process is symmetric under the transformation  $s \rightarrow 1 - s$ . This function is illustrated in Figure 3.

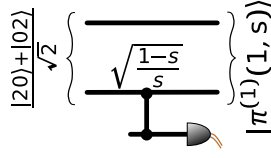


FIG. 2. The scheme for generating elementary variable primate state  $|\pi^{(1)}(1, s)\rangle$ .

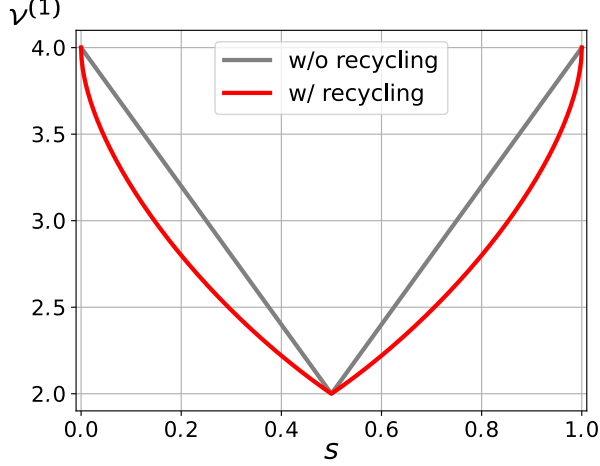


FIG. 3. The photon resource cost  $\nu^{(1)}$  for generating the elementary variable primate state  $|\pi^{(1)}(1, s)\rangle$ .

### B. Sequential Fusion

The sequential fusion of primate states results in the generation of a GHZ state. By utilizing the generalized primate state defined in (10), it then becomes possible to generate a more general GHZ-like states. We define the target GHZ-like states  $|\text{GHZ}_N(s)\rangle$  as:

$$|\text{GHZ}_N(s)\rangle = \sqrt{s}|10\rangle^N + \sqrt{1-s}|01\rangle^N, \quad (14)$$

where qubits are encoded in a dual-rail basis, with single-qubit states represented by the Fock states of a photon distributed across two modes.

Our objective is to generate these GHZ-like states through the fusion of primate states, as illustrated in Figure 4. Starting with initial primate states  $|\pi^{(1)}(1, s)\rangle$ , we sequentially fuse them to construct larger primate states with increasing photon numbers:

$$|\pi^{(n_1)}(\lambda_1, s_1)\rangle \otimes |\pi^{(n_2)}(\lambda_2, s_2)\rangle \rightarrow |\pi^{(n_1+n_2)}(\lambda', s')\rangle, \quad (15)$$

as shown in Figure 4a. Subsequently, upon obtaining the primate state with the appropriate photon number  $|\pi^{(N)}(\lambda, s)\rangle$ , we perform a fusion operation on its outermost modes, as depicted in Figure 4b. This final fusion step eliminates the junk component and heralds the successful preparation of the target GHZ-like state.

We now provide explicit formulae for the updated parameters  $s'$  and  $\lambda'$ , as well as the success probability

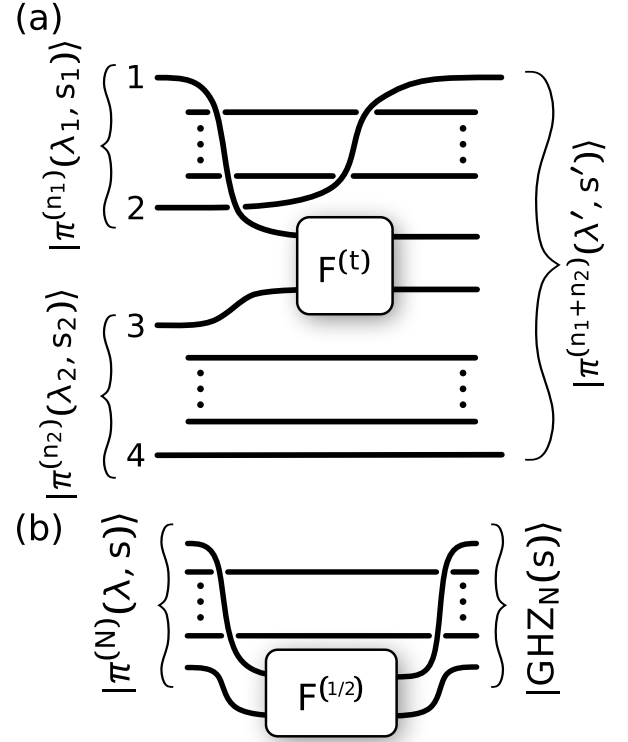


FIG. 4. (a) Example of two-primate fusion when the 13 mode pair is chosen for fusion. (b) The final fusion step that transforms a primate state into a GHZ-like state. Note that the final fusion is always optimal at a beamsplitter transmittance of 1/2.

of the fusion process (with detailed derivations in Appendix A). The new parameter  $s'$  depends on which pair of modes is chosen for fusion. There are two inequivalent cases:

$$s' = \begin{cases} \frac{s_1 s_2}{s_1 s_2 + (1-s_1)(1-s_2)}, & ij = 14 \text{ or } 23, \\ \frac{s_1(1-s_2)}{s_1(1-s_2) + (1-s_1)s_2}, & ij = 13 \text{ or } 24, \end{cases} \quad (16)$$

where the numbering corresponds to the labeling in Figure 4a. The success probability  $p_{ij}^{(1)}$  (the probability of measuring a single photon) also depends on the pair of modes  $ij$  being measured:

$$p_{14}^{(1)} = 2t(1-t) [s_1 \lambda_1 + (1-s_2) \lambda_2 - 2s_1(1-s_2)(1-t^2) \lambda_1 \lambda_2], \quad (17)$$

$$p_{13}^{(1)} = 2t(1-t) [s_1 \lambda_1 + s_2 \lambda_2 - 2s_1 s_2(1-t^2) \lambda_1 \lambda_2], \quad (18)$$

$$p_{23}^{(1)} = 2t(1-t) [(1-s_1) \lambda_1 + s_2 \lambda_2 - 2(1-s_1)s_2(1-t^2) \lambda_1 \lambda_2], \quad (19)$$

$$p_{24}^{(1)} = 2t(1-t) [(1-s_1) \lambda_1 + (1-s_2) \lambda_2 - 2(1-s_1)(1-s_2)(1-t^2) \lambda_1 \lambda_2]. \quad (20)$$

Using these expressions and the fact that the new  $\lambda'$  for

the state after successful fusion is fraction of the state  $|s'^{(n_1+n_2)}\rangle$  probability weight to  $p_{ij}^{(1)}$ :

$$\lambda' = \begin{cases} 2t(1-t)\lambda_1\lambda_2 \frac{s_1s_2+(1-s_1)(1-s_2)}{p_{ij}^{(1)}}, & ij = 14 \text{ or } 23 \\ 2t(1-t)\lambda_1\lambda_2 \frac{s_1(1-s_2)+(1-s_1)s_2}{p_{ij}^{(1)}}, & ij = 13 \text{ or } 24 \end{cases} \quad (21)$$

If the photon cost of generating  $|\pi^{(n_k)}(\lambda_k, s_k)\rangle$  is  $\nu^{(n_k)}$ , then we can derive the average photon cost of generating primate  $|\pi^{(n_1+n_2)}(\lambda', s')\rangle$  to be:

$$\nu^{(n_1+n_2)} = \frac{\nu^{(n_1)} + \nu^{(n_2)}}{p_{ij}^{(1)}}, \quad (22)$$

which carries on for latter fusions.

The final fusion step, shown in Figure 4b, transforms  $|\pi^{(N)}(\lambda, s)\rangle$  into the target state  $|\text{GHZ}_N(s)\rangle$  with a success probability given by:

$$p^{(1)} = 2t(1-t)\lambda. \quad (23)$$

It is straightforward to show that this fusion achieves its maximum success probability of  $\lambda/2$  when the beam-splitter transmittance is set to  $t = 1/2$ , as explicitly indicated in Figure 4b. Consequently, the second-to-last fusion, which produces the intermediate state  $|\pi^{(N)}(\lambda, s)\rangle$ , is most efficient when the product  $p_{ij}^{(1)}\lambda/2$  is maximized ( $p_{ij}^{(1)}$  being the probability of second-to-last fusion). From (21) we derive that this condition is also satisfied at  $t = 1/2$ .

Furthermore, the relationships in (16), rewritten in terms of  $s'^{-1} - 1$ , take the form:

$$(s'^{-1} - 1) = \begin{cases} (s_1^{-1} - 1)(s_2^{-1} - 1), & ij = 14 \text{ or } 23, \\ (s_1^{-1} - 1)/(s_2^{-1} - 1), & ij = 13 \text{ or } 24, \end{cases} \quad (24)$$

which provides a method for determining one of the very initial states  $|\pi^{(1)}(1, s)\rangle$  based on the target state  $|\text{GHZ}_N(s)\rangle$ .

When computing single-photon measurement probabilities, we summed the probabilities of the (01) and (10) outcomes for each fusion, even though these outcomes correspond to different resulting states. The rationale for this is that these states can be corrected (via a sign phase shift on a single mode) to yield the same state of the form  $|\pi^{(n_1+n_2)}(\lambda', s')\rangle$ . However, it is not necessary to actively correct the states during the outlined generation process. If corrections are not applied to the primates after each fusion, the resulting state will still be one that can subsequently be corrected to  $|\text{GHZ}_N(s)\rangle$  using phase shift determined by the outcomes of the fusion measurements. The correcting of the state may be avoided altogether by properly adjusting the processing of the fusion network [7].

Now functionally, there are two parameters we can tweak to arrive at the minimal photon resource cost. Those are the parameters  $s$  of the initial primates

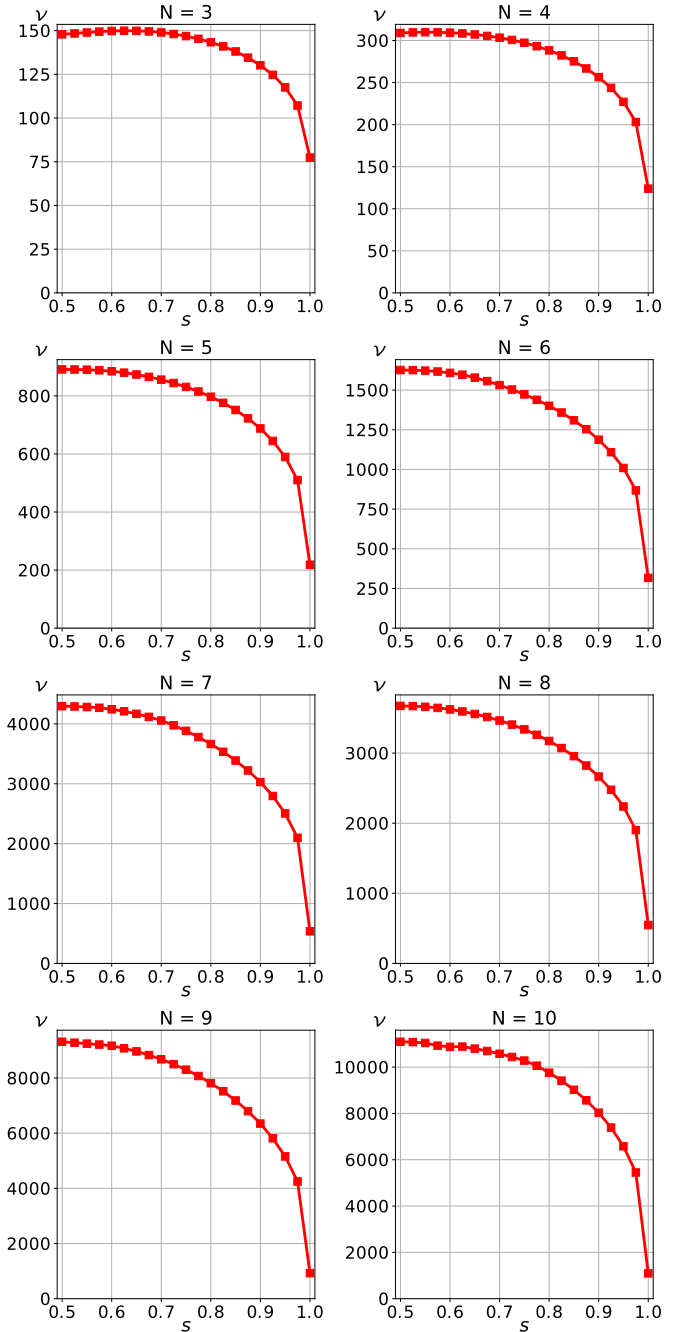


FIG. 5. Improved photon resource costs  $\nu$  for generating GHZ-like states with a variable parameter of entanglement  $s$  for different numbers of qubits  $N$  using fusion.

$|\pi^{(1)}(1, s)\rangle$  (which also affect  $\nu^{(1)}(s)$ ) and the transmissions of beam splitters  $t$  at each fusion  $F^{(t)}$ . But another degree of adaptability we are afforded is the actual path to arrive at the  $|\pi^{(N)}(\lambda, s)\rangle$  meaning which primates to fuse and how to fuse them. E.g., the two possible fusion sequences to get  $|\text{GHZ}_4\rangle$ -like states are:  $\{|\pi^{(1)}\rangle \otimes |\pi^{(1)}\rangle \rightarrow |\pi^{(2)}\rangle, |\pi^{(2)}\rangle \otimes |\pi^{(2)}\rangle \rightarrow |\pi^{(4)}\rangle \rightarrow |\text{GHZ}_4\rangle\}$  and  $\{|\pi^{(1)}\rangle \otimes |\pi^{(1)}\rangle \rightarrow |\pi^{(2)}\rangle, |\pi^{(2)}\rangle \otimes |\pi^{(1)}\rangle \rightarrow |\pi^{(3)}\rangle, |\pi^{(3)}\rangle \otimes |\pi^{(1)}\rangle \rightarrow |\pi^{(4)}\rangle \rightarrow |\text{GHZ}_4\rangle\}$ .



These fusion sequences correspond to addition chains for  $N$  [43]. An addition chain for  $N$  is a sequence of natural numbers where each term is the sum of two previous terms, with the sequence ending in  $N$ . We focus on a specific type known as star addition chains, in which one of the numbers being summed is always the immediate predecessor [44]. Notably, the minimal addition chain is guaranteed to be found among star chains if  $N < 12509$  [45], which comfortably covers the range of values relevant to practical implementations.

Since we lacked a method to determine the provably optimal fusion sequence without exhaustive testing, we considered all possible sequences and optimized the parameters  $t$  and  $s$  for each sequence individually. The results of this procedure are presented in Figure 5. From these results, we also observe that using primate states is not the absolute optimal generation strategy for all values of  $s$ . Naturally, at  $s = 1$ , no primate fusions are necessary because no superposition must be prepared, and the minimal average photon cost reduces to  $N$ . This limitation stems from the constraints inherent in using primate states, rather than employing all states achievable via linear optics.

A particularly noteworthy observation presented in Figure 6 is that even when targeting the maximally entangled state  $|\text{GHZ}_N(0.5)\rangle$ , employing variable intermediate primate states  $|\pi^{(1)}(1, s)\rangle$  yields better performance than using fixed non-variable primates  $|\pi^{(1)}(1, 0.5)\rangle$  (while still allowing  $t$  to vary). This can be explained by the fact that successful fusion probability explicitly depends on the  $s_i$  (17-20). The advantage of using variable primates for generating  $|\text{GHZ}_N(0.5)\rangle$  is showing from  $N \geq 7$  and grows with  $N$ . For example, at  $N = 7$  the cost improves by a miniscule amount from 4298.4 to 4296.0, and at  $N = 10$  from 11484.6 to 11093.5.

The fact that the resource demand for  $N = 7$  is greater than for  $N = 8$  can be partially explained by the fact that the addition chain for  $N = 7$  is longer:  $\{1, 2, 3, 5, 7\}$ , compared to  $\{1, 2, 4, 8\}$  for  $N = 8$ . Thus more fusions were required, which increased the demand. Notably, in each instance considered, the optimal fusion sequence was also one of the shortest, which is intuitive. However, we do not assert whether this will always be the case.

It is important to distinguish between two key performance metrics. In addition to the average photon number  $\nu$  required to generate a single GHZ state, we may also be interested in a probabilistic quantity: namely, the probability of successfully generating a GHZ state from  $2N$  photons using the primate-based approach. This corresponds to the single-pass probability that all primate fusions succeed simultaneously. We illustrate this in Figure 7, alongside the maximal possible single-pass probability for such a scheme, which is  $1/2^{2N-1}$  [46]. This demonstrates that the reduced photon resource cost is achieved at the expense of a lower single-pass success probability.

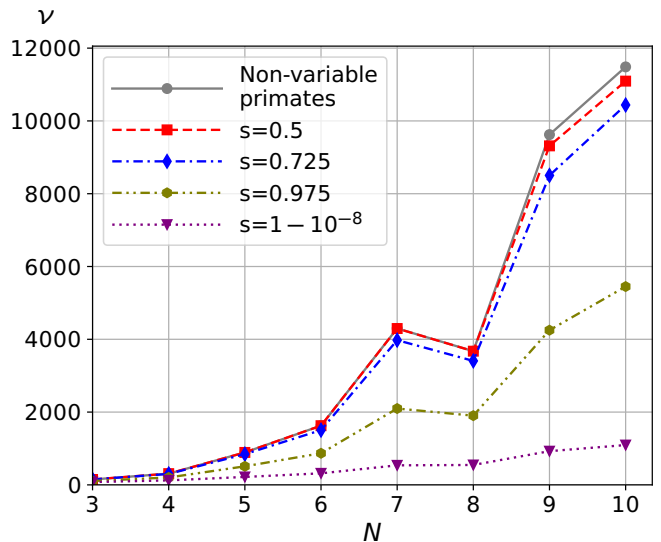


FIG. 6. Comparison of resource costs for generating the  $|\text{GHZ}_N(s)\rangle$  state. The gray line represents the procedure starting exclusively from  $|\pi^{(1)}(1, 0.5)\rangle$ , while other lines allow for variable initial primates.

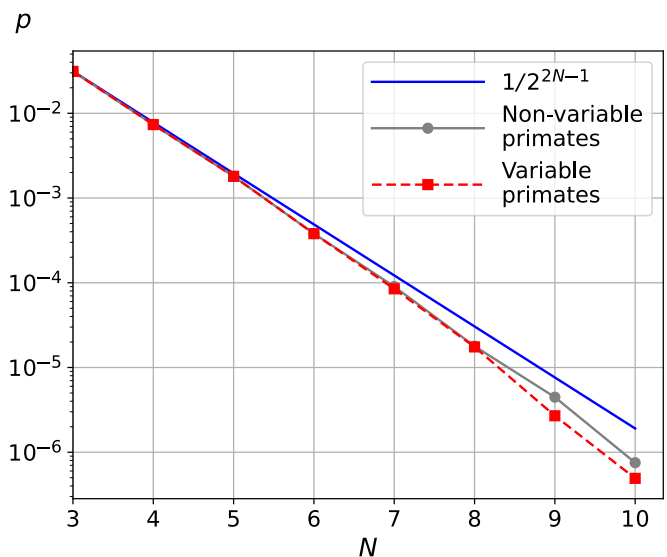


FIG. 7. Probability of generating a maximally entangled GHZ state from  $2N$  photons in a single pass. Depicted are the maximal achievable probability (which is  $1/2^{2N-1}$ ), along with the probabilities for resource-optimal schemes using both non-variable and variable primates.

#### IV. BLEEDING TECHNIQUE

Now, there is a more effective way to fuse two primates. Instead of using fusion unit  $F^{(t)}$  from Figure 1 to obtain  $|\pi^{(n_1+n_2)}(\lambda', s')\rangle$  from  $|\pi^{(n_1)}(\lambda_1, s_1)\rangle$  and  $|\pi^{(n_2)}(\lambda_2, s_2)\rangle$  we propose a new unit  $B^{(c)}$  based on bleeding [29]. A schematic depiction of the bleeding unit  $B^{(c)}$  is shown in Figure 8b. This unit consists of two subunits  $b^{(c)}$ ,

depicted in Figure 8a, which operate simultaneously until one succeeds. It is advantageous to bleed two pairs of modes simultaneously. These pairs are 14 & 23 or 13 & 24, with the difference between them affecting the resulting  $s'$  (as given in (16)). In principle, the fusion

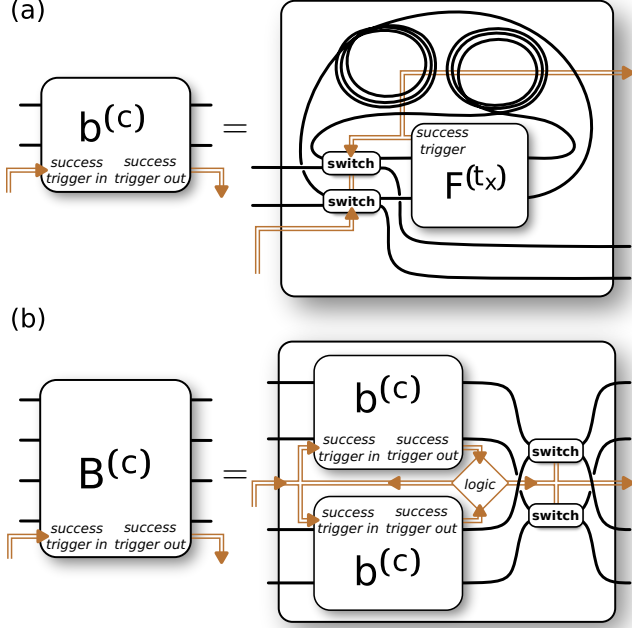


FIG. 8. Schematic depiction of the bleeding procedure units  $b^{(c)}$  and  $B^{(c)}$  is shown in (a) and (b), respectively. The switches in (a) default to passing and switch to crossing upon triggering. The configuration in (b) reroutes channels depending on which subunit  $b^{(c)}$  succeeds. The logical unit in (b) must be capable of discriminating between zero, one, or multiple photon measurements and, when necessary, send a triggering signal indicating success or failure terminating the bleeding procedure.

operations  $F^{(t_x)}$  should adjust the parameter  $t_x$  at each step, which can occur independently of the measurement results. This leads to the characterizing parameter  $c$ , defined as:

$$0 \leq c = \prod_{x=1}^{N_b} t_x^2 \leq 1, \quad (25)$$

which quantifies how exhaustive the  $N_b$  step bleeding process is. For example, given the number of bleeding steps  $N_b$  and choosing  $t_x = \sqrt{\frac{N_b+1-x}{N_b+2-x}}$ , we obtain  $c = \frac{1}{N_b+1} \xrightarrow{N_b \rightarrow \infty} 0$ . In the case of ideal bleeding we assume working in the large number of steps  $N_b \gg 1$  regime.

Tunability of  $t_x$  is, however, not strictly necessary. If the expected number of bleeding steps  $N_b$  is sufficiently large, one can instead choose a constant value, such as  $t_x = \sqrt[2N_b]{c}$ . In the ideal case of bleeding, the probability

of measuring two or more photons becomes vanishingly small due to  $t_x \approx 1$  for  $c > 0$ . For  $c = 0$ , one can set  $t_x = \sqrt[2N_b]{1/N_b}$ , which still satisfies  $t_x \approx 1$ .

Suppose an unsuccessful fusion attempt occurs during the first bleeding step of the pure primate states  $|\pi^{(n_1)}(\lambda_1, s_1)\rangle \otimes |\pi^{(n_2)}(\lambda_2, s_2)\rangle$ . It is straightforward to show that the state before the second bleeding step becomes  $|\pi^{(n_1)}(\frac{\lambda_1 t_1^2}{1-(1-t_1^2)\lambda_1}, s_1)\rangle \otimes |\pi^{(n_2)}(\frac{\lambda_2 t_2^2}{1-(1-t_2^2)\lambda_2}, s_2)\rangle$ , as derived in Appendix B. This indicates that the  $\lambda_i$  parameters are updated after the failed attempt. Consequently, the resulting state differs from the original, and we cannot expect the same  $\lambda'$  to be achieved in a successful second step as would have been obtained from a successful first step.

To address this issue, we introduce mixed primate states  $\pi^{(n)}(\lambda, s)$ , defined as:

$$\pi^{(n)}(\lambda, s) = \lambda |s^{(n)}\rangle \langle s^{(n)}| + (1-\lambda) |0\rangle \langle 0| \otimes \zeta \otimes |0\rangle \langle 0| + \dots \quad (26)$$

Here,  $\zeta$  represents the normalized density matrix of an  $n+1$  photon state in  $2n-2$  modes. The terms denoted by ellipsis correspond to off-diagonal contributions that do not affect probabilities and are eventually “measured out” during the generation of the target state. Since the state is mixed, the updated  $\lambda'$  can be calculated as an expectation value over all bleeding steps. This generalization offers a consistent framework for describing the state’s evolution under repeated bleeding attempts.

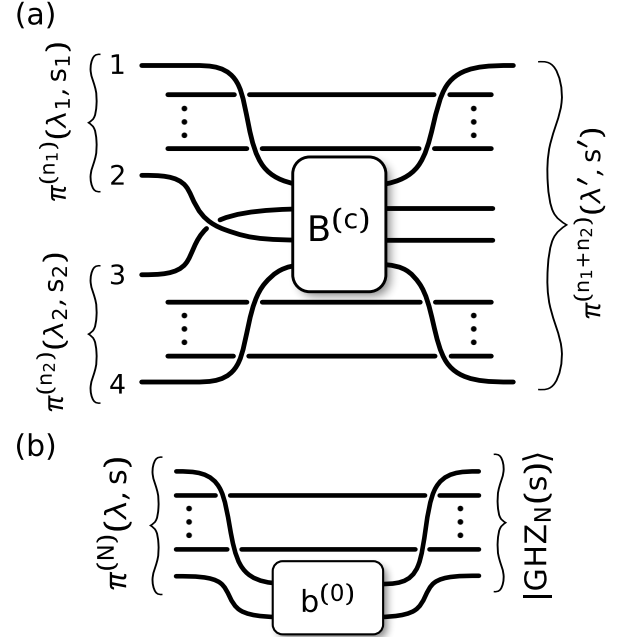


FIG. 9. (a) an example of two primate fusion when 13 & 24 mode pairs are chosen for interaction on unit  $B^{(c)}$ . (b) the final unit  $b^{(c)}$  that turns primate into the GHZ-like state. Notice that final  $b^{(c)}$  is always optimal at  $c = 0$ .

The sequential application of bleeding units is summarized in Figure 9. The fact that the application of  $b^{(0)}$

at  $\pi^{(N)}(\lambda, s)$  yields a pure state is obvious from (9, 26). In line with the previous section, one chooses the pairs of channels to interact on  $B^{(c)}$ . The success probability does not depend on  $s_i$  and is given by:

$$p^{(1)} = (1 - c)(\lambda_1 + \lambda_2 - (1 - c)\lambda_1\lambda_2). \quad (27)$$

If you choose to fuse the mode pairs 14 and 23, the resulting transformations are given by:

$$(s'^{-1} - 1) = (s_1^{-1} - 1)(s_2^{-1} - 1), \quad (28)$$

$$\lambda' = \frac{(s_1 s_2 + (1 - s_1)(1 - s_2))\lambda_1 \lambda_2 (1 + c)}{\lambda_1 + \lambda_2 - (1 - c)\lambda_1 \lambda_2}. \quad (29)$$

Alternatively, if you choose to fuse the mode pairs 13 and 24, the corresponding transformations are:

$$(s'^{-1} - 1) = (s_1^{-1} - 1)/(s_2^{-1} - 1), \quad (30)$$

$$\lambda' = \frac{(s_1(1 - s_2) + (1 - s_1)s_2)\lambda_1 \lambda_2 (1 + c)}{\lambda_1 + \lambda_2 - (1 - c)\lambda_1 \lambda_2}. \quad (31)$$

Detailed derivations of these formulae can be found in Appendix B. From these expressions, we can deduce that the success probability of the bleeding process increases as the parameter  $c$  decreases. However, a lower value of  $c$  leads to a decrease in the parameter  $\lambda'$ . This trade-off between success probability and the quality of the resulting state (as quantified by  $\lambda'$ ) introduces a non-trivial challenge in the choice of  $c$ .

Using the derived expressions, we optimize the initial parameters  $s$  of  $\pi^{(1)}(1, s)$  and the bleeding parameters  $c$  to minimize the average photon number cost  $\nu$  per  $|\text{GHZ}_N(s)\rangle$  state generation. Analogous to the process discussed in the previous section, one of the initial primates  $\pi^{(1)}(1, s)$  can be determined, and the parameter  $c$  can be fixed for specific bleeding units. We fix  $c = 0$  for the  $B^{(c)}$  unit that fuses two  $\pi^{(1)}(1, s)$  states. Similarly,  $c = 0$  is fixed for the final  $B^{(c)}$  unit that produces the state  $\pi^{(N)}(\lambda, s)$ , as well as for the last  $b^{(c)}$  that generates the desired  $|\text{GHZ}_N(s)\rangle$  state. This ensures that the final bleeding process is fully exhausted. These determinations of  $c$  simplify the optimization process by reducing the space of variables while maintaining resource efficiency. Figure 10 shows the average photon cost  $\nu$  for generating a single GHZ-like state as a function of the entanglement parameter  $s$  and the number of qubits  $N$  in the target state. To compare with the value  $N2^N$ , which represents the average photon cost demonstrated for GHZ state generation using the exhaustive bleeding method in [29], we plot the resource cost dependence on  $N$  for different target states in Figure 11. Our modified bleeding method also shows increasing advantage for generating the maximally entangled state  $|\text{GHZ}_N(0.5)\rangle$  as  $N$  grows. For example, at  $N = 4$  the cost improves from 64 to 63.7, and at  $N = 10$  from 10240 to 5287.6. In this case, utilizing variable primates does not yield better results when the target state is  $|\text{GHZ}_N(0.5)\rangle$ , as the optimization converges to non-variable initial primates  $|\pi^{(1)}(1, 0.5)\rangle$ .

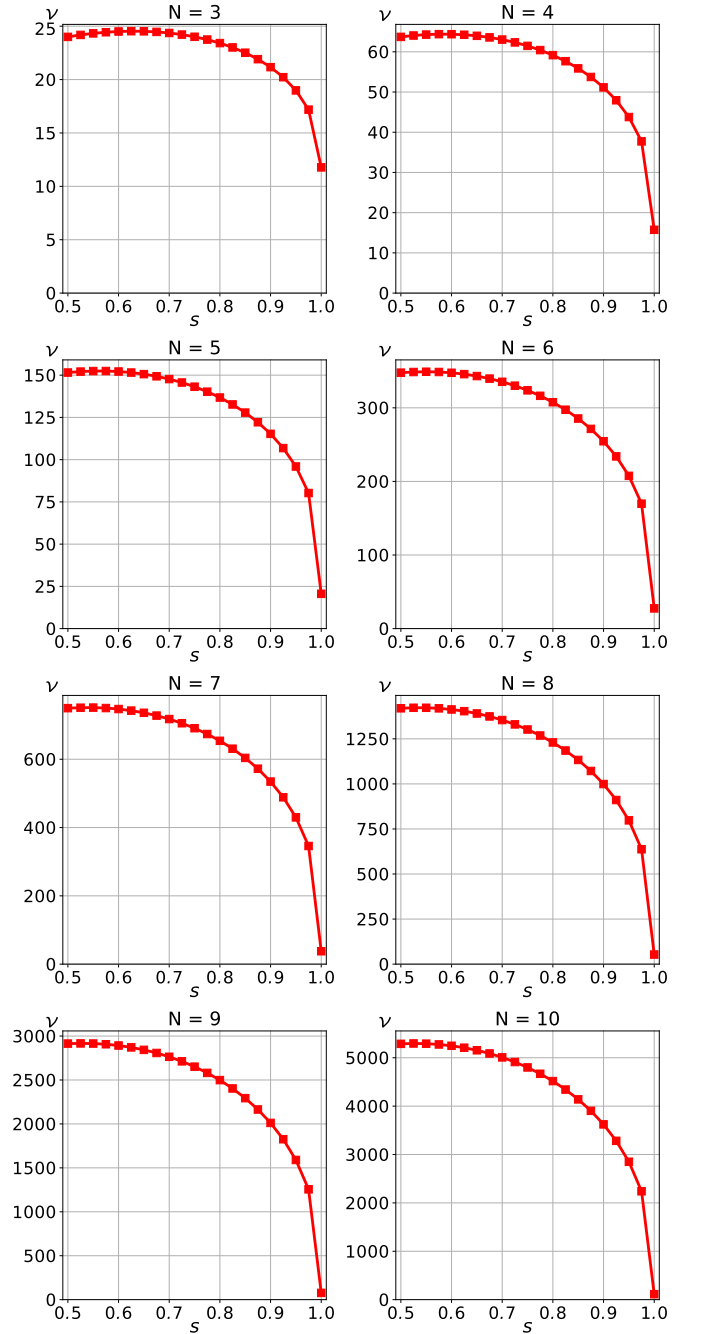


FIG. 10. Improved photon resource costs  $\nu$  for generating GHZ-like states with a variable parameter of entanglement  $s$  for different numbers of qubits  $N$  using bleeding.

Nevertheless, significant improvements are still achieved due to the introduced tunability of the bleeding process itself. Meaning that introduced non-exhaustive bleeding demonstrates advantage.

In contrast to the results in Section III, the optimal fusion sequence is not always the shortest. For instance, for  $N = 4$ , the sequence  $\{1, 2, 4\}$  has no variable  $c$  and yields a final resource cost of 64, while the sequence  $\{1, 2, 3, 4\}$  has one variable  $c$  (with an optimal value of 0.072) and



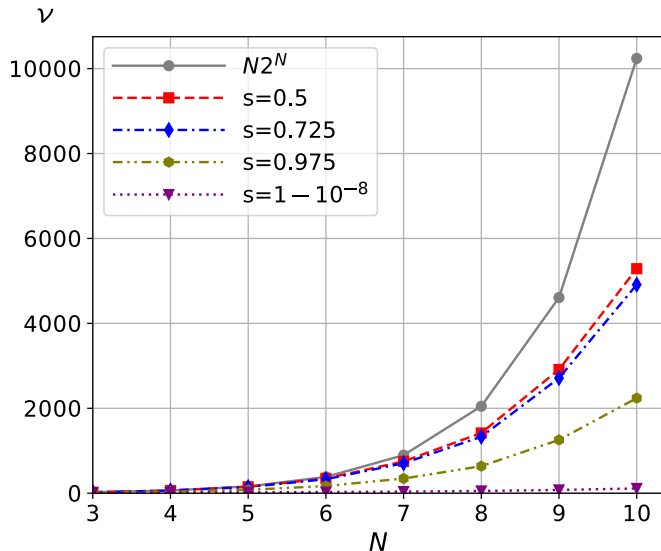


FIG. 11. Comparison of resource costs for generating  $|\text{GHZ}_N(s)\rangle$  using bleeding. The gray line shows the cost  $N2^N$  when initial primates are fixed and only exhaustive bleeding is employed, while other lines allow for variable primates and adjustable  $c$  in bleeding units.

yields a final resource cost of 63.7.

Again, the comparison of single-pass probability in Figure 12 showcases that the reduced photon resource cost comes at the expense of a lower single-pass success probability. We compare the maximal achievable single-pass probability for an exhaustive breeding scheme, which is  $1/2^{N-1}$  [29], with the single-pass probability of the proposed resource-optimal non-exhaustive breeding scheme.

It is noteworthy, when comparing Figure 6 and Figure 11, that as the number of qubits  $N$  increases, the advantage of bleeding for generating  $|\text{GHZ}_N(0.5)\rangle$  in comparison to using only fusion diminishes. However, even for  $N = 10$ , the bleeding method still provides up to twice the efficiency compared to approach in Section III.

## V. DISCUSSION

As shown in Figure 6, even when generating an  $N$  qubit GHZ state, using intermediate states with variable entanglement is more resource-efficient. Thus, our work demonstrates the utility of intermediate variable-entanglement states directly for established ways for photonic quantum computation. However, given the modest gains, it ultimately falls to the specific experimental setup to decide whether adopting a more complex generation scheme for  $|\pi^{(1)}(1, s)\rangle$  is justified over simply relying on maximally entangled primates  $|\pi^{(1)}(1, 0.5)\rangle$ . Concrete numerical evaluation of loss introduced along the complexification of a scheme is needed to evaluate experimental feasibility for photonic quantum computation [47, 48].

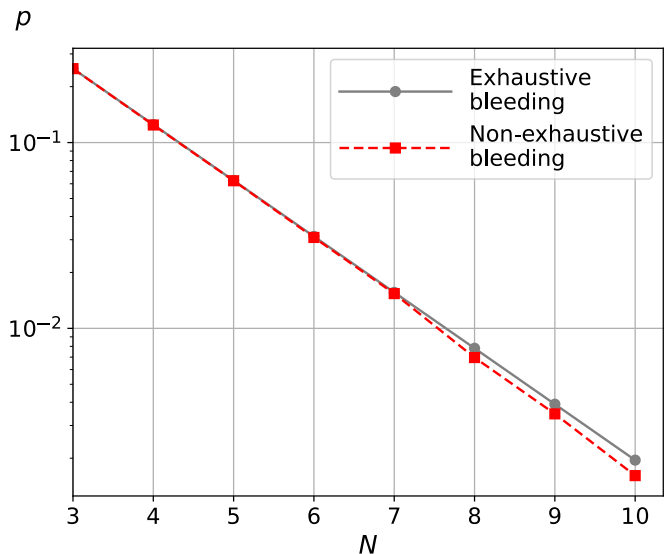


FIG. 12. Probability of generating a maximally entangled GHZ state from  $2N$  photons in a single pass. Depicted are the probability of exhaustive breeding (equal to  $1/2^{N-1}$ ), along with the probabilities for the resource-optimal scheme using non-exhaustive breeding.

In contrast, the results in Figure 11 show that non-exhaustive bleeding significantly outperforms the use of only exhaustive bleeding. In this case, the optimal generation of maximally entangled GHZ states does not require variable-entanglement primates, making the experimental implementation not substantially more difficult than the original proposal in [29]. We therefore encourage its adoption in experimental realizations of the bleeding method.

Our findings suggest there might be more efficient ways to generate maximally entangled GHZ states using other types of intermediate states. These new states could potentially offer lower resource requirements or higher success probabilities than current primate-based approaches. Investigating these alternatives (which may involve different photon distributions, mode encodings, or entanglement structures) could lead to more scalable and practical methods for photonic quantum information processing.

We have focused on using intermediate states with variable entanglement combined with maximally entangling fusion operations. An alternative strategy for producing target states with variable entanglement is to employ generalized, non-maximally entangling fusion — an approach recently explored in [49–51].

While GHZ-like states currently lack established applications in photonic quantum computation, we conjecture they may serve as valuable separate resources, such as for boosting established operations or other specialized tasks. For instance, a recent study demonstrates that these states, when supplemented with a single ancilla qubit, can be represented as stabilizer states [52].

## ACKNOWLEDGMENTS

S.A.F. acknowledges the support from the Foundation for the Advancement of Theoretical Physics and Mathematics (BASIS) (Project № 23-2-10-15-1) and the Scholarships of the President of the Russian Federation for postgraduate students.

- 
- [1] S. Aaronson and A. Arkhipov, The computational complexity of linear optics, *Theory of Computing* **9**, 143–252 (2013).
- [2] H.-S. Zhong, H. Wang, Y.-H. Deng, M.-C. Chen, L.-C. Peng, Y.-H. Luo, J. Qin, D. Wu, X. Ding, Y. Hu, P. Hu, X.-Y. Yang, W.-J. Zhang, H. Li, Y. Li, X. Jiang, L. Gan, G. Yang, L. You, Z. Wang, L. Li, N.-L. Liu, C.-Y. Lu, and J.-W. Pan, Quantum computational advantage using photons, *Science* **370**, 1460 (2020).
- [3] P. I. Sund, R. Uppu, S. Paesani, and P. Lodahl, Hardware requirements for realizing a quantum advantage with deterministic single-photon sources, *Phys. Rev. A* **109**, 042613 (2024).
- [4] D. E. Browne and T. Rudolph, Resource-efficient linear optical quantum computation, *Phys. Rev. Lett.* **95**, 010501 (2005).
- [5] K. Kieling, T. Rudolph, and J. Eisert, Percolation, renormalization, and quantum computing with nondeterministic gates, *Phys. Rev. Lett.* **99**, 130501 (2007).
- [6] M. Gimeno-Segovia, P. Shadbolt, D. E. Browne, and T. Rudolph, From three-photon Greenberger-Horne-Zeilinger states to ballistic universal quantum computation, *Phys. Rev. Lett.* **115**, 020502 (2015).
- [7] S. Bartolucci, P. Birchall, H. Bombín, H. Cable, C. Dawson, M. Gimeno-Segovia, E. Johnston, K. Kieling, N. Nickerson, M. Pant, F. Pastawski, T. Rudolph, and C. Sparrow, Fusion-based quantum computation, *Nature Communications* **14**, 912 (2023).
- [8] H. Bombín, C. Dawson, R. V. Mishmash, N. Nickerson, F. Pastawski, and S. Roberts, Logical blocks for fault-tolerant topological quantum computation, *PRX Quantum* **4**, 020303 (2023).
- [9] D. Litinski and N. Nickerson, Active volume: An architecture for efficient fault-tolerant quantum computers with limited non-local connections, (2022), [arXiv:2211.15465 \[quant-ph\]](https://arxiv.org/abs/2211.15465).
- [10] A. Avanesov, A. Shurinov, I. Dyakonov, and S. Straupe, Building a fusion-based quantum computer using teleported gates, *Quantum* **9**, 1762 (2025).
- [11] Y. L. Lim, A. Beige, and L. C. Kwek, Repeat-until-success linear optics distributed quantum computing, *Phys. Rev. Lett.* **95**, 030505 (2005).
- [12] M. Gimeno-Segovia, T. Rudolph, and S. E. Economou, Deterministic generation of large-scale entangled photonic cluster state from interacting solid state emitters, *Phys. Rev. Lett.* **123**, 070501 (2019).
- [13] P. Dhara, S. J. Johnson, C. N. Gagatsos, P. G. Kwiat, and S. Guha, Heralded multiplexed high-efficiency cascaded source of dual-rail entangled photon pairs using spontaneous parametric down-conversion, *Phys. Rev. Appl.* **17**, 034071 (2022).
- [14] P. Hilaire, L. Vidro, H. S. Eisenberg, and S. E. Economou, Near-deterministic hybrid generation of arbitrary photonic graph states using a single quantum emitter and linear optics, *Quantum* **7**, 992 (2023).
- [15] S. C. Wein, T. G. de Brugière, L. Music, P. Senellart, B. Bourdoncle, and S. Mansfield, Minimizing resource overhead in fusion-based quantum computation using hybrid spin-photon devices, (2024), [arXiv:2412.08611 \[quant-ph\]](https://arxiv.org/abs/2412.08611).
- [16] L. A. Pettersson, A. S. Sørensen, and S. Paesani, Deterministic generation of concatenated graph codes from quantum emitters, *PRX Quantum* **6**, 010305 (2025).
- [17] Z. Aqua and B. Dayan, Atom-mediated deterministic generation and stitching of photonic graph states, *PRX Quantum* **6**, 010340 (2025).
- [18] E. Knill, R. Laflamme, and G. J. Milburn, A scheme for efficient quantum computation with linear optics, *Nature* **409**, 46–52 (2001).
- [19] E. Knill, Quantum gates using linear optics and postselection, *Phys. Rev. A* **66**, 052306 (2002).
- [20] I. Forbes, F. Ghafari, E. Deacon, S. P. P. Singh, E. Lavie, P. Yard, R. Shaw, A. Laing, and N. Tischler, Heralded generation of entanglement with photons, *Rep. Prog. Phys.* **88**, 086002 (2025).
- [21] N. N. Skryabin, Y. A. Biriukov, M. A. Dryazgov, S. A. Fldzhyan, S. A. Zhuravitskii, A. S. Argenchiev, I. V. Kondratyev, L. A. Tsoma, K. I. Okhlopov, I. M. Gruzinov, A. Y. Arsenyev, K. V. Taratorin, M. Y. Saygin, I. V. Dyakonov, M. V. Rakhlin, A. I. Galimov, G. V. Klimko, S. V. Sorokin, I. V. Sedova, M. M. Kulagina, Y. M. Zadiranov, A. A. Toropov, S. A. Evlashin, A. A. Korneev, S. P. Kulik, and S. S. Straupe, Heralded generation of programmable two-qubit entangled states on a linear-optical platform, *Optica Quantum* **3**, 162 (2025).
- [22] S. Chen, L.-C. Peng, Y.-P. Guo, X.-M. Gu, X. Ding, R.-Z. Liu, J.-Y. Zhao, X. You, J. Qin, Y.-F. Wang, Y.-M. He, J. J. Renema, Y.-H. Huo, H. Wang, C.-Y. Lu, and J.-W. Pan, Heralded three-photon entanglement from a single-photon source on a photonic chip, *Phys. Rev. Lett.* **132**, 130603 (2024).
- [23] S. A. Fldzhyan, M. Y. Saygin, and S. P. Kulik, Compact linear optical scheme for Bell state generation, *Phys. Rev. Res.* **3**, 043031 (2021).
- [24] S. A. Fldzhyan, M. Y. Saygin, and S. P. Kulik, Programmable heralded linear optical generation of two-qubit states, *Phys. Rev. Appl.* **20**, 054030 (2023).
- [25] F. V. Gubarev, I. V. Dyakonov, M. Y. Saygin, G. I. Struchalin, S. S. Straupe, and S. P. Kulik, Improved heralded schemes to generate entangled states from single photons, *Phys. Rev. A* **102**, 012604 (2020).
- [26] F. V. Gubarev, Fock space perspective on optimal heralding schemes, (2021), [arXiv:2108.09336 \[quant-ph\]](https://arxiv.org/abs/2108.09336).
- [27] A. Chernikov, S. S. Sysoev, E. A. Vashukevich, and T. Y.

- Golubeva, Heralded gate search with genetic algorithms for quantum computation, *Phys. Rev. A* **108**, 012609 (2023).
- [28] G. S. Hartnett, D. Kielpinski, S. Maity, P. S. Mundada, Y. Baum, and M. R. Hush, Automated discovery of heralded ballistic graph state generators for fusion-based photonic quantum computation (2025), [arXiv:2508.16505 \[quant-ph\]](#).
- [29] S. Bartolucci, P. M. Birchall, M. Gimeno-Segovia, E. Johnston, K. Kieling, M. Pant, T. Rudolph, J. Smith, C. Sparrow, and M. D. Vidrighin, Creation of entangled photonic states using linear optics (2021), [arXiv:2106.13825 \[quant-ph\]](#).
- [30] S. Paesani, J. F. F. Bulmer, A. E. Jones, R. Santagati, and A. Laing, Scheme for universal high-dimensional quantum computation with linear optics, *Phys. Rev. Lett.* **126**, 230504 (2021).
- [31] B. Pankovich, A. Neville, A. Kan, S. Omkar, K. H. Wan, and K. Bradler, Flexible entangled-state generation in linear optics, *Phys. Rev. A* **110**, 032402 (2024).
- [32] D. Bhatti and S. Barz, Heralding higher-dimensional bell and Greenberger–Horne–Zeilinger states using multipoint splitters, *New J. Phys.* **27**, 033006 (2025).
- [33] J. Clausen, M. Dakna, L. Knoell, and D. G. Welsch, Conditional quantum state engineering at beam splitter arrays, *Acta Physica Slovaca* **49**, 653 (1999).
- [34] Y. I. Bogdanov, K. G. Katamadze, G. V. Avosopiants, L. V. Belinsky, N. A. Bogdanova, A. A. Kalinkin, and S. P. Kulik, Multiphoton subtracted thermal states: Description, preparation, and reconstruction, *Physical Review A* **96** (2017).
- [35] T. Hayrynen, J. Oksanen, and J. Tulkki, Exact theory for photon subtraction for fields from quantum to classical limit, *EPL (Europhysics Letters)* **87**, 44002 (2009).
- [36] P. Marek, J. Provaznık, and R. Filip, Loop-based subtraction of a single photon from a traveling beam of light, *Opt. Express* **26**, 29837 (2018).
- [37] C. Cohen-Tannoudji, B. Diu, and F. Laloe, Creation and annihilation operators for identical particles, in *Quantum Mechanics, Volume 3: Fermions, Bosons, Photons, Correlations, and Entanglement*, Vol. 3 (Wiley-VCH, 2020) Chap. XV, pp. 1591–1616, 1st ed.
- [38] M. Reck, A. Zeilinger, H. J. Bernstein, and P. Bertani, Experimental realization of any discrete unitary operator, *Phys. Rev. Lett.* **73**, 58 (1994).
- [39] Y.-P. Guo, G.-Y. Zou, X. Ding, Q.-H. Zhang, M.-C. Xu, R.-Z. Liu, J.-Y. Zhao, Z.-X. Ge, L.-C. Peng, K.-M. Xu, Y.-Y. Lou, Z. Ning, L.-J. Wang, H. Wang, Y.-H. Huo, Y.-M. He, C.-Y. Lu, and J.-W. Pan, Boosted fusion gates above the percolation threshold for scalable graph-state generation (2024), [arXiv:2412.18882 \[quant-ph\]](#).
- [40] N. Hauser, M. J. Bayerbach, S. E. D’Aurelio, R. Weber, M. Santandrea, S. P. Kumar, I. Dhand, and S. Barz, Boosted Bell-state measurements for photonic quantum computation, *npj Quantum Information* **11**, 41 (2025).
- [41] K. Kieling, *Linear optics quantum computing – construction of small networks and asymptotic scaling*, *PhD Thesis*, Imperial College London (2008).
- [42] G. de Glinasty, P. Bagourd, S. Draux, and B. Bourdoncle, Simple rules for two-photon state preparation with linear optics, in *2024 IEEE International Conference On Quantum Computing And Engineering, Qce, Vol 1* (IEEE, Los Alamitos, 2025) p. 706–711.
- [43] P. Downey, B. Leong, and R. Sethi, Computing sequences with addition chains, *SIAM Journal on Computing* **10**, 638 (1981).
- [44] A. Brauer, On addition chains, *Bulletin of the American Mathematical Society* (1939).
- [45] D. E. Knuth, *The Art of Computer Programming*, 3rd ed., Vol. 2 (Addison–Wesley, 1997) Section 4.6.3.
- [46] M. Gimeno-Segovia, *Towards practical linear optical quantum computing*, *PhD Thesis*, Imperial College London (2015).
- [47] A. Melkozerov, A. Avanesov, I. Dyakonov, and S. Straupe, Analysis of optical loss thresholds in the fusion-based quantum computing architecture, *APL Quantum* **1**, 036119 (2024).
- [48] F. H. B. Somhorst and J. J. Renema, Mitigating quantum operation infidelity through engineering the distribution of photon losses, (2025), [arXiv:2507.04805 \[quant-ph\]](#).
- [49] F. Schmidt and P. van Loock, Generalized fusions of photonic quantum states using static linear optics (2024), [arXiv:2410.20261 \[quant-ph\]](#).
- [50] N. Rimock, K. Cohen, and Y. Oz, Generalized type II fusion of cluster states, (2024), [arXiv:2406.15666 \[quant-ph\]](#).
- [51] A. A. Melkozerov, M. Y. Saygin, and S. S. Straupe, Entanglement-efficiency trade-offs in the fusion-based generation of photonic GHZ-like states (2025), [arXiv:2507.12389 \[quant-ph\]](#).
- [52] H. Zakaryan, K.-R. Revis, and Z. Raissi, Nonsymmetric Greenberger-Horne-Zeilinger states: Weighted hypergraph and controlled-unitary graph representations, *Physical Review A* **112** (2025).

## Appendix A: Fusion

In this section we derive formulae from Section III. We investigate the fusion of  $|\pi^{(n_1)}(\lambda_1, s_1)\rangle \otimes |\pi^{(n_2)}(\lambda_2, s_2)\rangle$ . Consider a case when a single photon is measured upon fusion of the 23 mode pair. Focusing on the (10) measurement

and carefully enumerating the terms in the superposition. Starting with the  $|s^{(n_1)}\rangle \otimes |s^{(n_2)}\rangle$  term:

$$\begin{aligned} \hat{\mathcal{M}}_{23}^{(10)} |s^{(n_1)}\rangle \otimes |s^{(n_2)}\rangle = & \sqrt{\frac{t\hat{\mathcal{N}}_{23}(1-t)}{2}} (\hat{a}_2 + \hat{a}_3) (\sqrt{s_1}|2\rangle_1|01\rangle^{n_1-1}|0\rangle_2 + \sqrt{1-s_1}|0\rangle_1|10\rangle^{n_1-1}|2\rangle_2) \otimes \\ & \otimes (\sqrt{s_2}|2\rangle_3|01\rangle^{n_2-1}|0\rangle_4 + \sqrt{1-s_2}|0\rangle_3|10\rangle^{n_2-1}|2\rangle_4) = \\ & \sqrt{t(1-t)} \left( \left[ \sqrt{s_1 s_2} |2\rangle_1 |01\rangle^{n_1+n_2-1} |0\rangle_4 + \sqrt{(1-s_1)(1-s_2)} |0\rangle_1 |10\rangle^{n_1+n_2-1} |2\rangle_4 \right] + \right. \\ & \left. \sqrt{t^2(1-s_1)s_2} |0\rangle_1 |10\rangle^{n_1-1} (|12\rangle_{23} + |21\rangle_{23}) |01\rangle^{n_2-1} |0\rangle_4 \right). \quad (\text{A1}) \end{aligned}$$

The term in square brackets is proportional to the state  $|s'^{(n_1+n_2)}\rangle$ , with the updated parameter:

$$s' = \frac{s_1 s_2}{s_1 s_2 + (1-s_1)(1-s_2)}. \quad (\text{A2})$$

The other types of terms are:

$$\begin{aligned} \hat{\mathcal{M}}_{23}^{(10)} |s^{(n_1)}\rangle \otimes |0\rangle_3 |\zeta_2\rangle |0\rangle_4 = & \sqrt{\frac{t\hat{\mathcal{N}}_{23}(1-t)}{2}} (\hat{a}_2 + \hat{a}_3) (\sqrt{s_1}|2\rangle_1|01\rangle^{n_1-1}|0\rangle_2 + \sqrt{1-s_1}|0\rangle_1|10\rangle^{n_1-1}|2\rangle_2) |0\rangle_3 |\zeta_2\rangle |0\rangle_4 = \\ & \sqrt{t(1-t)(1-s_1)} |0\rangle_1 |10\rangle^{n_1} |\zeta_2\rangle |0\rangle_4 \quad (\text{A3}) \end{aligned}$$

$$\begin{aligned} \hat{\mathcal{M}}_{23}^{(10)} |0\rangle_1 |\zeta_1\rangle |0\rangle_2 \otimes |s^{(n_2)}\rangle = & \sqrt{\frac{t\hat{\mathcal{N}}_{23}(1-t)}{2}} (\hat{a}_2 + \hat{a}_3) |0\rangle_1 |\zeta_1\rangle |0\rangle_2 (\sqrt{s_2}|2\rangle_3|01\rangle^{n_2-1}|0\rangle_4 + \sqrt{1-s_2}|0\rangle_3|10\rangle^{n_2-1}|2\rangle_4) = \\ & \sqrt{t(1-t)s_2} |0\rangle_1 |\zeta_1\rangle |01\rangle^{n_2} |0\rangle_4 \quad (\text{A4}) \end{aligned}$$

To compute the success probability  $p^{(1)}$ , we sum the probabilities of all terms, appropriately weighted by  $\lambda_1$  and  $\lambda_2$ . Accounting for both the (10) and (01) cases (which only differ by the sign in the superposition) with a factor of 2, we find:

$$\begin{aligned} p^{(1)} = 2t(1-t) (\lambda_1 \lambda_2 (s_1 s_2 + (1-s_1)(1-s_2)) + 2t^2(1-s_1)s_2) + \lambda_1(1-\lambda_2)(1-s_1) + (1-\lambda_1)\lambda_2 s_2 = \\ 2t(1-t) (\lambda_1(1-s_1) + \lambda_2 s_2 - 2(1-t^2)(1-s_1)s_2 \lambda_1 \lambda_2), \quad (\text{A5}) \end{aligned}$$

and the  $\lambda'$  is determined by the ratio of the probability weight of the  $|s^{(n_1+n_2)}\rangle$  state to the total success probability:

$$\lambda' = \frac{t(1-t)\lambda_1\lambda_2(s_1s_2 + (1-s_1)(1-s_2))}{p^{(1)}/2}. \quad (\text{A6})$$

By following a similar procedure, we can derive analogous expressions for any other fused mode pairs.

## Appendix B: Bleeding

In this section we derive formulae in Section IV. We begin by considering a product state of two primates, denoted as  $\pi^{(n_1)}(\lambda_1, s_1) \otimes \pi^{(n_2)}(\lambda_2, s_2)$ , where each primate is defined as:

$$\pi^{(n_i)}(\lambda_i, s_i) = \lambda_i |s_i^{(n_i)}\rangle \langle s_i^{(n_i)}| + (1-\lambda_i) |0\rangle \langle 0| \otimes \zeta_i \otimes |0\rangle \langle 0| + \dots \quad (\text{B1})$$

To reiterate:  $\zeta_i$  represents the normalized density matrix of an  $n_i + 1$  photon state in  $2n_i$  modes, while the terms denoted by ellipsis correspond to off-diagonal contributions that do not influence probabilities. For simplicity, we omit ellipsis in subsequent derivations.

As discussed in the main text, we propose performing the bleeding operation simultaneously on two pairs of modes — e.g. the innermost and the outermost 23 and 14. Let  $t_x$  denote the fusion units' parameters at the  $x$ -th bleeding step. As discussed in the main text, we propose performing the bleeding operation simultaneously on two pairs of modes — for instance, the innermost and outermost pairs 23 and 14. After a single bleeding step, there are two key measurement outcomes of interest: the projection operator for the case where zero photons are measured (given by (8)) and the case where one photon is measured (given by (9)). Since a single bleeding unit  $B^{(c)}$  consists of two subunits  $b^{(c)}$ , which operate simultaneously, we must apply an additional zero-photon measurement operator for each case to account for the evolution of the state.

*a. Case 1: No Photon Detected*

If no photons are detected during the  $(x+1)$ -th bleeding step, the resulting state is:

$$\begin{aligned} \hat{\mathcal{M}}_{14}^{(\text{vac})} \hat{\mathcal{M}}_{23}^{(\text{vac})} \pi_1(\lambda_1(x), s_1) \otimes \pi_2(\lambda_2(x), s_2) \hat{\mathcal{M}}_{14}^{\dagger(\text{vac})} \hat{\mathcal{M}}_{23}^{\dagger(\text{vac})} = \\ \left( \lambda_1(x) t_{x+1}^2 |s_1^{(n_1)}\rangle \langle s_1^{(n_1)}| + (1 - \lambda_1(x)) |0\rangle \langle 0|_1 \otimes \zeta_1 \otimes |0\rangle \langle 0|_2 \right) \\ \otimes \left( \lambda_2(x) t_{x+1}^2 |s_2^{(n_2)}\rangle \langle s_2^{(n_2)}| + (1 - \lambda_2(x)) |0\rangle \langle 0|_3 \otimes \zeta_2 \otimes |0\rangle \langle 0|_4 \right), \quad (\text{B2}) \end{aligned}$$

where  $\lambda_i(x)$  denotes the parameter values after the  $x$ -th unsuccessful step, with  $\lambda_i(0) = \lambda_i$ . The probability of this outcome is:

$$p_{x+1}^{(0)} = (1 - (1 - t_{x+1}^2) \lambda_1(x)) (1 - (1 - t_{x+1}^2) \lambda_2(x)), \quad (\text{B3})$$

where  $p_x^{(0)}$  denotes the probability that no photons have been measured in the first  $x$  steps. The updated parameters  $\lambda_1(x+1)$  and  $\lambda_2(x+1)$  are then:

$$\lambda_i(x+1) = \frac{\lambda_i(x) t_{x+1}^2}{1 - (1 - t_{x+1}^2) \lambda_i(x)}, \quad (\text{B4})$$

These expressions can be simplified. The probability of no detection up to and including the  $x$ -th step is:

$$p_x^{(0)} = \left( 1 - \left( 1 - \prod_{x'=1}^x t_{x'}^2 \right) \lambda_1 \right) \left( 1 - \left( 1 - \prod_{x'=1}^x t_{x'}^2 \right) \lambda_2 \right), \quad (\text{B5})$$

and the updated parameters after the  $x$ -th step are:

$$\lambda_i(x) = \frac{\lambda_i \prod_{x'=1}^x t_{x'}^2}{1 - \left( 1 - \prod_{x'=1}^x t_{x'}^2 \right) \lambda_i}. \quad (\text{B6})$$

*b. Case 2: Single Photon Detected*

We now consider the case where a single photon is detected in one of the four modes after propagation through the fusion units. We fix the bleeding step  $x$  at which this measurement occurs. Specifically, suppose a (10) outcome is observed for the 23 mode pair, while vacuum is detected on 14. The effect of this measurement on the pure state  $|s_1^{(n_1)}\rangle |s_2^{(n_2)}\rangle$  is given by:



$$\begin{aligned}
\hat{\mathcal{M}}_{14}^{(\text{vac})} \hat{\mathcal{M}}_{23}^{(10)} |s_1^{(n_1)}\rangle |s_2^{(n_2)}\rangle &= \sqrt{\frac{t_x^{\hat{\mathcal{N}}_{14} + \hat{\mathcal{N}}_{23}} (1 - t_x)}{2}} (\hat{a}_2 + \hat{a}_3) \cdot \\
&\cdot (\sqrt{s_1} |2\rangle_1 |01\rangle^{n_1-1} |0\rangle_2 + \sqrt{1-s_1} |0\rangle_1 |10\rangle^{n_1-1} |2\rangle_2) (\sqrt{s_2} |2\rangle_3 |01\rangle^{n_2-1} |0\rangle_4 + \sqrt{1-s_2} |0\rangle_3 |10\rangle^{n_2-1} |2\rangle_4) = \\
&\sqrt{t_x^3 (1 - t_x)} \left( \left[ \sqrt{s_1 s_2} |2\rangle_1 |01\rangle^{n_1+n_2-1} |0\rangle_4 + \sqrt{(1-s_1)(1-s_2)} |0\rangle_1 |10\rangle^{n_1+n_2-1} |2\rangle_4 \right] + \right. \\
&\quad \left. + \sqrt{(1-s_1)s_2} |0\rangle_1 |10\rangle^{n_1-1} (|21\rangle_{23} + |12\rangle_{23}) |01\rangle^{n_2-1} |0\rangle_4 \right). \quad (\text{B7})
\end{aligned}$$

The state in square brackets is proportional to the new state  $|s'^{(n_1+n_2)}\rangle$ , where

$$s' = \frac{s_1 s_2}{s_1 s_2 + (1-s_1)(1-s_2)} \Rightarrow (s'^{-1} - 1) = (s_1^{-1} - 1) (s_2^{-1} - 1). \quad (\text{B8})$$

There are four possible single-photon measurement outcomes from fusing the 14 and 23 pairs, all of which can be corrected via simple phase shifts or mode permutations to yield the same final state structure. From (B7), the weight  $\lambda'_x$  of the resulting  $|s'^{(n_1+n_2)}\rangle$  state after step  $x$  is:

$$\lambda'_x = 4\lambda_1(x-1)\lambda_2(x-1)t_x^3(1-t_x) \frac{s_1 s_2 + (1-s_1)(1-s_2)}{p_x^{(1)}}, \quad (\text{B9})$$

where the factor  $\lambda_1(x-1)\lambda_2(x-1)$  arises from the probability of the component  $|s_1^{(n_1)}\rangle\langle s_1^{(n_1)}| \otimes |s_2^{(n_2)}\rangle\langle s_2^{(n_2)}|$  in the input  $\pi_1 \otimes \pi_2$ , and  $p_x^{(1)}$  is the total probability of detecting a single photon at step  $x$ , including contributions from terms involving  $\zeta_1$  or  $\zeta_2$ . While the full expression for  $p_x^{(1)}$  is not needed for subsequent derivations, we provide it for completeness:

$$\begin{aligned}
p_x^{(1)} &= 2t_x(1-t_x) (\lambda_1(x-1) + \lambda_2(x-1) - 2(1-t_x^2)\lambda_1(x-1)\lambda_2(x-1)) = \\
&= \frac{2t_x(1-t_x) \prod_{x'=1}^{x-1} t_{x'}^2 \left( \lambda_1 + \lambda_2 - 2 \left( 1 - \prod_{x'=1}^x t_{x'}^2 \right) \lambda_1 \lambda_2 \right)}{p_{x-1}^{(0)}}. \quad (\text{B10})
\end{aligned}$$

### 1. Continuum Approximation

At its core, the bleeding process assumes that  $t_x \approx 1$  for most steps. To simplify the analysis, we approximate the discrete transmission steps with a continuous representation, letting  $t_x \approx 1 - \Delta(x)dx \approx e^{-\Delta(x)dx}$ . Using this approximation, we focus only on terms up to the first power of  $dx$ . This allows us to derive from (B4) differential equations describing the evolution of  $\lambda_1(x)$  and  $\lambda_2(x)$ :

$$\lambda_i(x+dx) = \lambda_i(x)(1 - 2\Delta(x)dx)(1 + 2\Delta(x)dx\lambda_i(x)) \Rightarrow \dot{\lambda}_i(x) = -2\Delta(x)\lambda_i(x)(1 - \lambda_i(x)), \quad (\text{B11})$$

with the solution:

$$\lambda_i(x) = \frac{1}{1 + \frac{1-\lambda_i(0)}{\lambda_i(0)} e^{2 \int_0^x \Delta(x') dx'}} = \frac{\lambda_i e^{-2 \int_0^x \Delta(x') dx'}}{1 - \left( 1 - e^{-2 \int_0^x \Delta(x') dx'} \right) \lambda_i}, \quad (\text{B12})$$

which equals to (B6) if  $e^{-2 \int_0^x \Delta(x') dx'} = \prod_{x'=1}^x t_{x'}^2$ . The probability of not measuring any photons at step  $x$  from (B3) can be approximated to be:

$$p^{(0)}(x) = e^{-2\Delta(x)(\lambda_1(x) + \lambda_2(x))dx}, \quad (\text{B13})$$

and the cumulative probability of not measuring any photons up to step  $x$  is:

$$p^{(0)}(< x) = e^{-2 \int_0^x \Delta(x') (\lambda_1(x') + \lambda_2(x')) dx'} = \left(1 - \left(1 - e^{-2 \int_0^x \Delta(x') dx'}\right) \lambda_1\right) \left(1 - \left(1 - e^{-2 \int_0^x \Delta(x') dx'}\right) \lambda_2\right). \quad (\text{B14})$$

The value of  $\lambda'(x)$  at step  $x$  is approximated from (B9) to be:

$$\lambda'(x) = 4\lambda_1(x)\lambda_2(x)\Delta(x)dx \frac{s_1s_2 + (1-s_1)(1-s_2)}{dp^{(1)}(x)}, \quad (\text{B15})$$

where it is emphasized that probability of measuring single photon  $dp^{(1)}(x)$  in the vicinity of  $x$  is proportional to  $dx$ .

Our main interest lies in determining  $\lambda'$  for the final state after the entire bleeding process. Due to the nature of the density matrix formalism, this reduces to an expectation value:

$$\lambda' = \frac{1}{p^{(1)}} \int_0^\infty \lambda'(x)p^{(0)}(< x)dp^{(1)}(x) = \frac{4(s_1s_2 + (1-s_1)(1-s_2))}{p^{(1)}} \int_0^\infty \lambda_1(x)\lambda_2(x)\Delta(x)p^{(0)}(< x)dx. \quad (\text{B16})$$

With bleeding success probability  $p^{(1)}$  given by:

$$p^{(1)} = 1 - p^{(0)}(< \infty), \quad (\text{B17})$$

because probability of measuring 2 or more photons is of higher order on  $dx$ . Remarkably, these integrals can be evaluated analytically, yielding the key results:

$$(s'^{-1} - 1) = (s_1^{-1} - 1)(s_2^{-1} - 1), \quad (\text{B18})$$

$$p^{(1)} = (1 - c)(\lambda_1 + \lambda_2 - (1 - c)\lambda_1\lambda_2) \quad (\text{B19})$$

$$\lambda' = (s_1s_2 + (1-s_1)(1-s_2)) \frac{\lambda_1\lambda_2(1+c)}{\lambda_1 + \lambda_2 - (1-c)\lambda_1\lambda_2}, \quad (\text{B20})$$

$$c = e^{-2 \int_0^\infty \Delta(x) dx} \approx \prod_{x=1}^{N_b} t_x^2, \quad (\text{B21})$$

where we have used  $\lambda_i = \lambda_i(0)$ . The parameter  $c$  represents the strength of the bleeding procedure: the closer  $c$  is to 0, the more exhaustive the bleeding is. Alternatively, if we fuse pairs 13 and 24 instead of 14 and 23, the expressions change:

$$(s'^{-1} - 1) = (s_1^{-1} - 1)/(s_2^{-1} - 1), \quad (\text{B22})$$

$$\lambda' = (s_1(1-s_2) + (1-s_1)s_2) \frac{\lambda_1\lambda_2(1+c)}{\lambda_1 + \lambda_2 - (1-c)\lambda_1\lambda_2}. \quad (\text{B23})$$

With the help of the fact that  $\frac{\lambda_1 + \lambda_2}{2\lambda_1\lambda_2} \geq 1$ , it can be easily proven that  $\frac{dp^{(1)}}{dc} \leq 0$  and  $\frac{d\lambda'}{dc} \geq 0$ . Consequently, optimizing  $c$  requires balancing these competing effects to minimize the overall resource cost.

We have used a continuum approximation because it yielded a neat single parameter  $c$  that governs a perfect bleeding behavior with infinite number of steps and transmissions arbitrarily close to 1. For reference here are the exact expressions when no such assumptions are made:

$$p^{(1)} = \sum_{x=1}^{N_b} 2t_x(1-t_x) \left( \lambda_1 + \lambda_2 - 2 \left(1 - \prod_{x'=1}^x t_{x'}^2\right) \lambda_1\lambda_2 \right) \prod_{x'=1}^{x-1} t_{x'}^2, \quad (\text{B24})$$

$$\lambda' = 4\lambda_1\lambda_2 \frac{s_1s_2 + (1-s_1)(1-s_2)}{p^{(1)}} \sum_{x=1}^{N_b} t_x^3(1-t_x) \prod_{x'=1}^{x-1} t_{x'}^4, \quad (\text{B25})$$

where summation goes up to the number of bleeding steps  $N_b$ . If other mode pairs are fused then  $s_1(1-s_2) + (1-s_1)s_2$  is substituted instead of  $s_1s_2 + (1-s_1)(1-s_2)$ .